

# PCCP

Accepted Manuscript



This is an *Accepted Manuscript*, which has been through the Royal Society of Chemistry peer review process and has been accepted for publication.

*Accepted Manuscripts* are published online shortly after acceptance, before technical editing, formatting and proof reading. Using this free service, authors can make their results available to the community, in citable form, before we publish the edited article. We will replace this *Accepted Manuscript* with the edited and formatted *Advance Article* as soon as it is available.

You can find more information about *Accepted Manuscripts* in the [Information for Authors](#).

Please note that technical editing may introduce minor changes to the text and/or graphics, which may alter content. The journal's standard [Terms & Conditions](#) and the [Ethical guidelines](#) still apply. In no event shall the Royal Society of Chemistry be held responsible for any errors or omissions in this *Accepted Manuscript* or any consequences arising from the use of any information it contains.

## Characterization of an abnormal photoluminescence behavior upon crystal-phase transition of perovskite $\text{CH}_3\text{NH}_3\text{PbI}_3$

Weiguang Kong,<sup>a</sup> Zhenyu Ye,<sup>a</sup> Zhen Qi,<sup>b</sup> Bingpo Zhang,<sup>a</sup> Miao Wang,<sup>a</sup> Arash Rahimi-Iman,<sup>c</sup> Huizhen Wu<sup>a\*</sup>

<sup>a</sup> Department of Physics and State Key Laboratory of Silicon Materials, Zhejiang University, Hangzhou, Zhejiang 310027, P.R. China

<sup>b</sup> State Key Laboratory for Infrared Physics, Shanghai Institute of Technical Physics, Chinese Academy of Sciences, 200083, Shanghai, P. R. China

<sup>c</sup> Faculty of physics & Material sciences center, Philipps University Marburg, D-35032 Marburg, Germany

**Abstract:** *Solution-processed hybrid perovskite of  $\text{CH}_3\text{NH}_3\text{PbI}_3$  ( $\text{MAPbI}_3$ ) exhibits an abnormal luminescent behavior at around the tetragonal-orthorhombic phase transition temperature. The combination of time resolved photoluminescence (PL), variable excitation power PL, and variable-temperature X-ray diffraction (XRD) allows us to clearly interpret the abnormal luminescent features in the phase transition region of  $\text{MAPbI}_3$ . Both PL and XRD results unambiguously prove the coexistence of the tetragonal and orthorhombic phase of  $\text{MAPbI}_3$  in the temperature range of 150 to 130 K. The two luminescent features observed in orthorhombic phase at  $T < 130$  K originate*

---

\* Address correspondence to Huizhen Wu, Department of Physics and State Key Laboratory of Silicon Materials, Zhejiang University, Hangzhou, Zhejiang 310027, P.R. China. E-mail: hzhu@zju.edu.cn.

*from free excitons and donor-acceptor-pair (DAP) transitions, respectively.*

*The comprehensive understanding of optical properties upon phase transition in MAPbI<sub>3</sub> will benefit the development of new optoelectronic devices.*

**Keyword:** perovskite, CH<sub>3</sub>NH<sub>3</sub>PbI<sub>3</sub>, TRPL, phase transition

## 1. Introduction

Novel light-harvesting materials for mesoscopic solar cells such as CH<sub>3</sub>NH<sub>3</sub>PbX<sub>3</sub> (X: Cl, Br, I) have attracted much attention, following the pioneering work on organic-inorganic hybrid perovskites.[1-6] Particularly, a breakthrough on the methylammonium (CH<sub>3</sub>NH<sub>3</sub>: MA) lead iodide (thereafter denoted as MAPbI<sub>3</sub>) perovskite was achieved recently, when the energy conversion efficiency of the hybrid perovskites photovoltaic devices was found to reach up to 19.3%.[1] Further studies suggest that MAPbI<sub>3</sub> crystals can become even promising for lasing applications.[7-10] According to previous reports,[8, 11] tetragonal MAPbI<sub>3</sub> exhibits a broad PL band around its band-gap energy of ~1.6 eV. As temperature (*T*) decreases, tetragonal MAPbI<sub>3</sub> transforms into an orthorhombic phase along with an abnormal emission blue-shift. Such orthorhombic MAPbI<sub>3</sub> possesses two emission features. Wehrenfennig et al.[12] and Wu et al.[13] assigned the two emission features to the phase coexistence of orthorhombic and tetragonal phases. However, Fang et al.[14] and Xing et al.[7] attributed the two features to bound-exciton and free-exciton emissions. No consensus has been reached because of insufficient experimental evidence,

especially concerning the underlying physical mechanisms in the phase transition  $T$  region. Although the symmetry and electronic structures of MAPbI<sub>3</sub> crystals have been widely studied,[15-19] these results could hardly be used to interpret the optical properties of the orthorhombic MAPbI<sub>3</sub> because of little consideration of the impact of crystal defects involved. Since the optical properties of a semiconductor material are related to both intrinsic and extrinsic properties, PL spectroscopy is a highly sensitive and useful tool to assess both the intrinsic, e.g., band structure, excitons, and defects, and extrinsic features, such as impurities. Indeed, a comprehensive understanding of the optical properties of the orthorhombic MAPbI<sub>3</sub> is required in order to expand the application fields of MAPbI<sub>3</sub> and to develop new optoelectronic devices based on this material system.[14]

In this work, time resolved PL (TRPL) and variable-excitation-power PL characterizations are performed to study the luminescent features of MAPbI<sub>3</sub> in different  $T$  regions. Moreover, the crystalline phase structures of the MAPbI<sub>3</sub> crystal are also characterized by variable-temperature X-ray diffraction (XRD). Our results clarify the origin of the two PL features of orthorhombic MAPbI<sub>3</sub>. As  $T$  is between 150 and 130 K, these two PL features are attributed to the phase coexistence of tetragonal and orthorhombic phases with different band-gap energies. As  $T$  falls below 130 K, the two PL features are dominated by the donor-acceptor pair (DAP) recombinations. We conclude that the tetragonal-orthorhombic phase transition for the solution-processed MAPbI<sub>3</sub> is

a gradual process which is related to the defects in the crystal.

## 2. Experimental section

**2.1 CH<sub>3</sub>NH<sub>3</sub>I Synthesis.** CH<sub>3</sub>NH<sub>3</sub>I was synthesized by reacting 30 mL of methylamine (40% in methanol, TCI) and 32.3 mL of hydroiodic acid (57 wt% in water, Aldrich) in a 250 mL round-bottom flask at 0 °C for 2 h with stirring. The precipitate was recovered by putting the solution on a rotary evaporator and carefully removing the solvents at 50 °C. The yellowish raw product methylammonium iodide (CH<sub>3</sub>NH<sub>3</sub>I) was washed with diethyl ether by stirring the solution for 30 min, a step which was repeated three times, and finally recrystallized from a mixed solvent of diethyl ether and ethanol. After filtration, the solid was collected and dried at 60 °C in a vacuum oven for 24 h.

**2.2 MAPbI<sub>3</sub> Synthesis.** The film of MAPbI<sub>3</sub> on Si substrate was formed by dropping a 40 wt% precursor solution of equimolar CH<sub>3</sub>NH<sub>3</sub>I and PbI<sub>2</sub> in  $\gamma$ -butyrolactone onto the Si wafer which was firstly hydrophilic treated by the aqueous solution of H<sub>2</sub>O<sub>2</sub> and NH<sub>4</sub>OH with volume ratio of H<sub>2</sub>O<sub>2</sub>:NH<sub>4</sub>OH:H<sub>2</sub>O=1:1:5 for 30 min. The film formation was realized by spin-coating at 1500 rpm for 30 s, and then 2500 rpm for 40 min in air. The film coated on the Si wafer led to the change of color upon drying at room temperature, indicating the formation of MAPbI<sub>3</sub> in the solid state. The MAPbI<sub>3</sub> film was annealed in air for 15 min at 100 °C.

**2.3 Characterization.** The MAPbI<sub>3</sub> film was characterized by X-ray diffraction (XRD) on a PANalytical x-ray diffractometer (Model EMPYREAN) with a

monochromatic Cu  $K_{\alpha 1}$  radiation. The lattice parameters were precisely determined using Si powders as the internal standard reference material. Steady-state and time-resolved PL spectra were measured by an Edinburgh FLS920 spectroscopy system, using laser excitation at 405 nm. Scanning electron microscopy (SEM) characterization was carried out with a Hitachi S4800 operating at an acceleration voltage of 5 kV.

### 3. Results and discussion

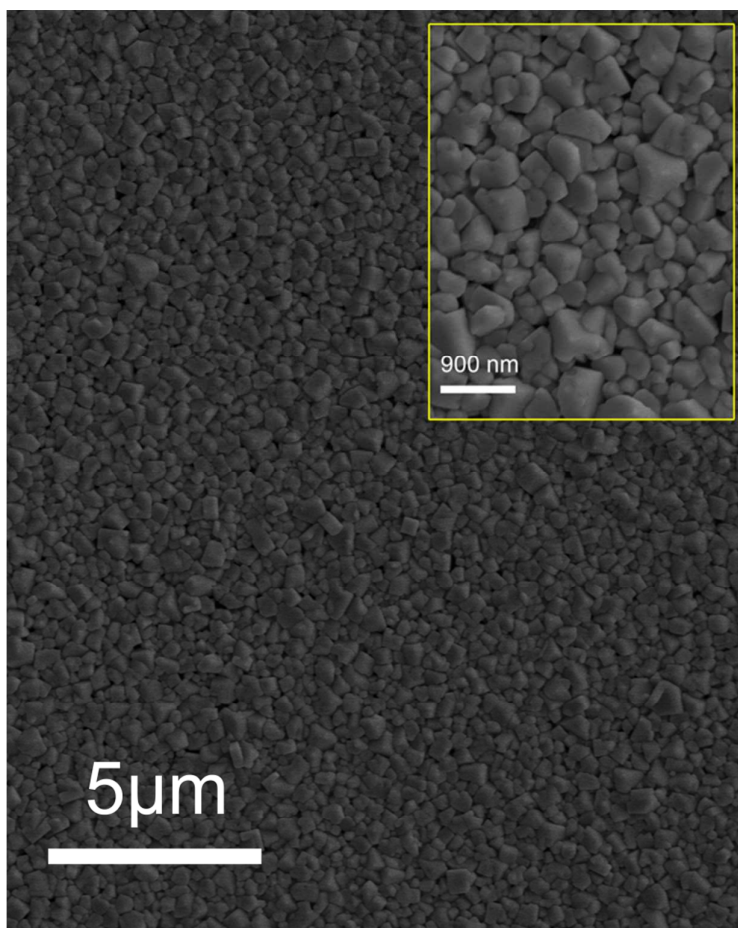


Figure 1 A top view SEM image showing the surface morphology of the MAPbI<sub>3</sub> film. Inset is the enlarged graph for clear observation of the grain size and shape.

It is known that surface morphology influence on the luminescence features and dynamics of crystal materials. Proper control of the crystalline shape and size could be essential for random lasers.[20, 21] Figure 1 shows the top view SEM of the as-prepared MAPbI<sub>3</sub> film with distinct crystal grains. It is seen that the grain sizes of MAPbI<sub>3</sub> are between 100-500 nm, similar to the previous reported one.[22] The SEM confirms that the film is conformal and spatially homogeneous. This helps one exclude the random signals during the following PL measurements.

Figure 2(a-b) present the PL spectra acquired for the MAPbI<sub>3</sub> perovskite-crystal film at temperatures between 300 K and 10 K in steps of 10 K (A detailed picture of temperature-dependent PL can be found in Figure S1). As shown in Figure 2(a), the maximum of the PL band (labeled 'Peak\_T') in tetragonal MAPbI<sub>3</sub>, which is due to the near-band-edge (NBE) transition,[8, 11, 12] locates at 783 nm (1.58 eV) at room temperature. NBE here is to note that the PL of MAPbI<sub>3</sub> at variable temperatures could come from the free carrier or free exciton recombination, as Yamada and his coworkers [23, 24] found that the exciton binding energy of MAPbI<sub>3</sub> could change from ~30 meV at 13 K to 6 meV at 300 K, and the excitons could be dissociated by thermal energy at high temperatures. The location of the PL band agrees well with the latest experimental results which have proved that the band-gap energy of tetragonal MAPbI<sub>3</sub> is ~1.60 eV, [8, 11-14, 23] rather than 1.5 eV as predicted by theoretical computation. It has been widely accepted in the work related to the

area of solar cells.[25-30] Peak\_T exhibits a continuous red-shift as  $T$  decreases from 300 K to 140 K, which is contrary to typical semiconductors and may be due to the change in material parameters. With a further decline in  $T$ , Peak\_T begins to blue shift, leading to the feature at lower temperatures labeled 'Peak\_O<sub>II</sub>' in Figure 2(b). This fact is in accordance with the observation of variations in the absorption edge of the MAPbI<sub>3</sub>. [12, 31] In contrast to the tetragonal phase, the orthorhombic MAPbI<sub>3</sub> possesses two PL features, marked as Peak\_O<sub>I</sub> and Peak\_O<sub>II</sub>, as shown in Figure 2(b). With the decrease in  $T$ , Peak\_O<sub>I</sub> shows a monotonous red shift throughout the whole low temperature range, while Peak\_O<sub>II</sub> initially blue-shifts ( $140 > T > 80$  K) and thereafter red-shifts ( $T < 80$  K). This complex variation in Peak\_O<sub>II</sub> was also noted in the literature by other groups.[12-14] Here, the strain effect of different substrates on the PL properties of MAPbI<sub>3</sub> can be ruled out, since the MAPbI<sub>3</sub> grown on different substrates, such as glass,[12, 14] quartz,[13] and Si, features similar PL behavior. The intricate variation of the PL spectra observed in the low temperature range is hence attributed to an inherent characteristic of the orthorhombic MAPbI<sub>3</sub>.



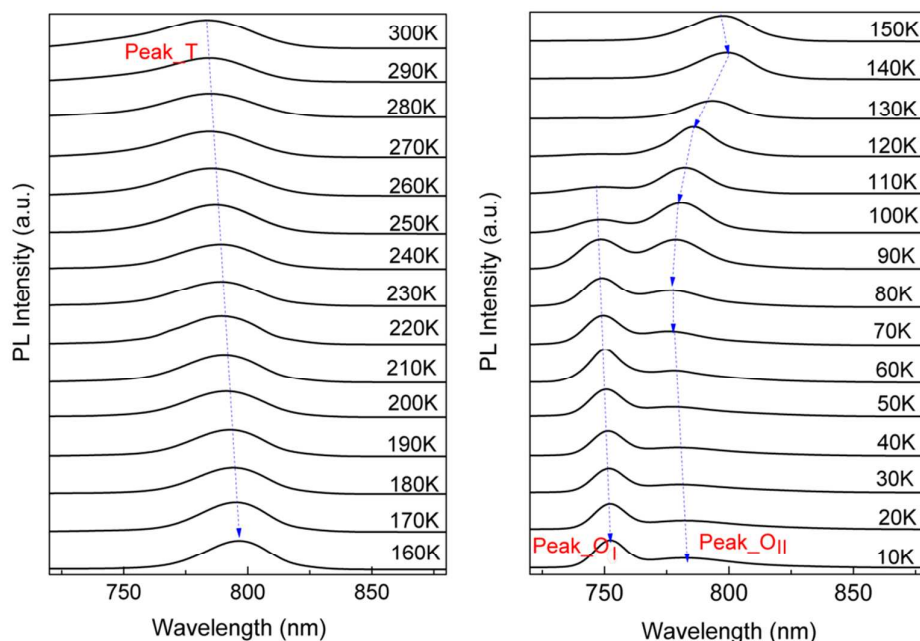


Figure 2 PL spectra of the MAPbI<sub>3</sub> perovskite-crystal film at variable temperatures, the arrows indicate the evolution of the maximum of the PL band: (a) MAPbI<sub>3</sub> in tetragonal phase and (b) MAPbI<sub>3</sub> in orthorhombic phase.

Since the orthorhombic MAPbI<sub>3</sub> is a direct-band-gap crystal,[17, 18, 30] multiple PL peaks indicate that there are multiple radiative recombination centers involved, e.g., intrinsic defect states, extrinsic impurities, and residual tetragonal MAPbI<sub>3</sub> crystals, etc. As mentioned in the **introduction**, there are two different viewpoints on the origin of Peak\_O<sub>II</sub>: (1) the inclusion of the tetragonal phase[11, 13] and (2) bound-state excitons in orthorhombic MAPbI<sub>3</sub>.<sup>12</sup> However, the origin of the continuous variations in PL resulting from the phase transition was disregarded. In order to solve this problem, TRPL is performed at three typical temperatures around the phase transition

temperature, ranging from 150 to 100 K. Figure 3(a-c) shows TRPL spectra of the MAPbI<sub>3</sub> perovskite at different time delays after the excitation pulse, where the dashed lines denote the shift of the emission peaks. The TRPL spectra of the MAPbI<sub>3</sub> measured at high temperatures are also provided in Figure S2 for comparison. As shown in Figure S2, there are no obvious emission energy shifts with time delay after excitation in tetragonal MAPbI<sub>3</sub>. This observation is consistent with previous reports on the homogeneously broadened emission line width of tetragonal MAPbI<sub>3</sub>.<sup>[8, 24]</sup> By contrast, at 140 K, Peak\_O<sub>II</sub> slightly red-shifts with time after excitation, indicating a different emission mechanism from that of Peak\_T. As  $T$  further decreases, a more evident red-shift in Peak\_O<sub>II</sub> is observed. This observation suggests that there is a migration of photo-excited carriers to lower energy sites as a function of time delay after a pulsed excitation. The evident temporal redshift in Peak\_O<sub>II</sub> at 120 K coincides well with a DAP recombination behavior. The photon energy and the recombination rate of the DAP-related emission are determined by the following equations, respectively:

$$\hbar\omega = E_g - E_A - E_D + e^2/(4\pi\epsilon_0\epsilon R) \quad (1)$$

$$1/\tau_{DA} \propto \exp[-2(R/\alpha_{D,A})] \quad (2)$$

where  $E_g$  is the band-gap energy,  $\epsilon_0$  is the static dielectric constant and  $E_D$  and  $E_A$  are the donor and acceptor binding energies, respectively;  $R$  is the distance between ionized donors and acceptors;  $(\tau_{DA})^{-1}$  and  $\alpha_{D,A}$  are the radiative recombination rate and the larger Bohr-radius equivalent of the donor and

acceptor, respectively. Thus, the emission energy ( $\hbar\omega$ ) from the spatially close pairs is higher than that from the spatially distant pairs because of the larger Coulomb interactions for the former. In addition, the electron-hole recombination probability for close pairs is higher than that for distant pairs because of greater wave function overlap. Therefore, the recombination rate for the high-energy transition is larger than that for the low-energy transition, which results in faster decay times for the photons with shorter wavelengths in the PL band.[32] The wavelength-dependent PL lifetimes measured at different  $T$  are illustrated in Figure 3(d). The lifetimes are obtained by fitting tri-exponential decay functions. The difference between the lifetimes on the long and short wavelength side is gradually increased from <50 ns at 140 K to 270 ns at 120 K. We thus conclude that Peak\_O<sub>II</sub> is due to the DAP recombination at  $T < 120$  K. As  $T$  is in the range of 140 to 120 K, the MAPbI<sub>3</sub> is in a transition state where two phases coexist. The TRPL spectra demonstrate that the transition from Peak\_T (NBE recombination) to Peak\_O<sub>II</sub> (DAP recombination) is a gradual process. The gradually increased red shift in Peak\_O<sub>II</sub> with a decrease in  $T$  can be interpreted as the decreased content of the tetragonal inclusions in host orthorhombic MAPbI<sub>3</sub>. Herein, we propose that Peak\_O<sub>I</sub> is the NBE emission of the orthorhombic MAPbI<sub>3</sub>, i.e., free exciton recombination due to the large binding energy at low temperature range as discussed above. This can be explained as follows: On the one side, the emission energy of Peak\_O<sub>I</sub> locates at 740-750 nm (as shown in Figure 2(b)), which is close to the absorption

maximum of orthorhombic  $\text{MAPbI}_3$  (740-760 nm).[31] On the other side, after a pulsed excitation, no time-dependent emission-energy shift can be observed, which is similar to the case of Peak\_T in tetragonal  $\text{MAPbI}_3$ .

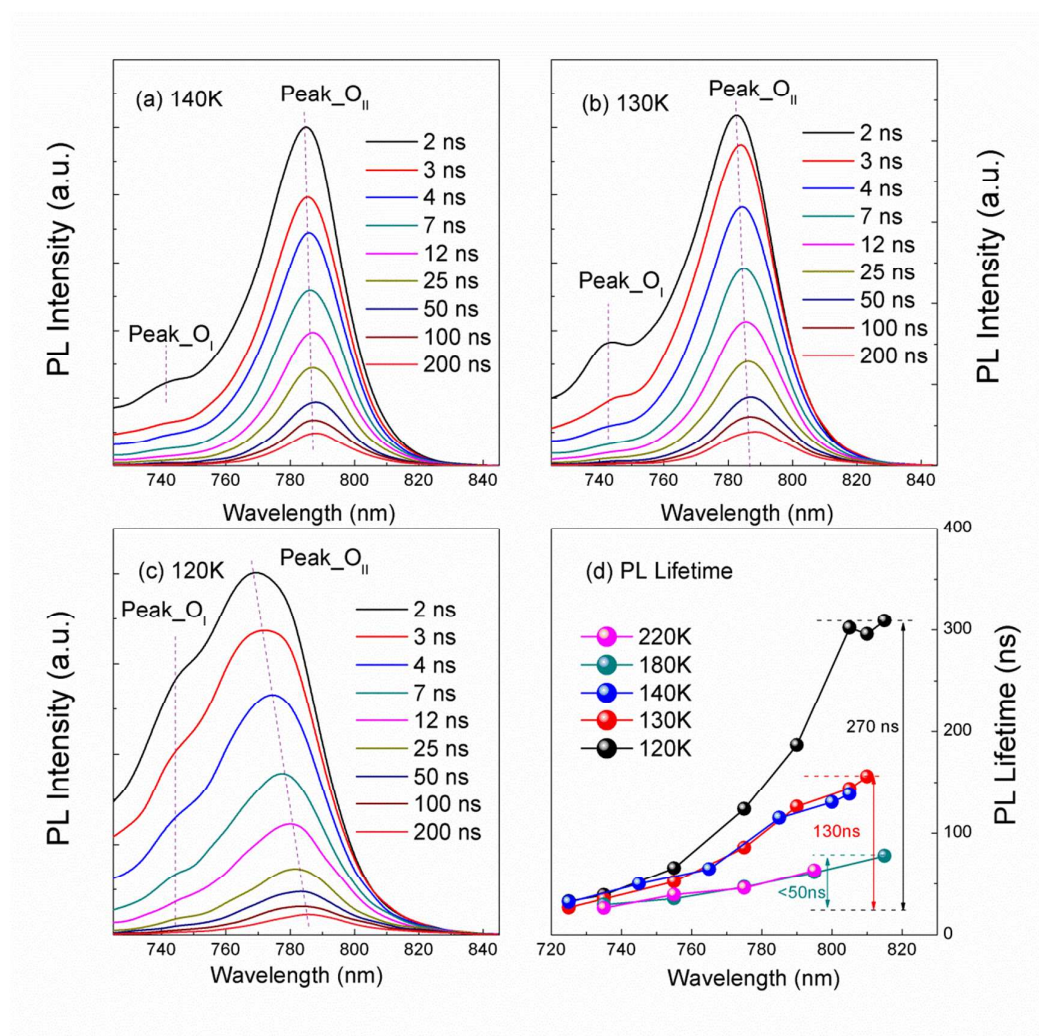


Figure 3 TRPL spectra of the  $\text{MAPbI}_3$  measured at (a) 140K, (b) 130K, and (c) 120K. (d) Wavelength dependent PL lifetimes of the  $\text{MAPbI}_3$  at different temperatures.

Tetragonal inclusions in the orthorhombic phase of  $\text{MAPbI}_3$  can potentially trap photo-excited excitons due to the narrower band gap of tetragonal  $\text{MAPbI}_3$  crystals than orthorhombic.[18, 33] Thus, a large density of free excitons could

agglomerate and eventually recombine within these inclusions.[12] This proposal can be supported by the fast quenching (within less than 10 nanoseconds) of Peak<sub>O<sub>I</sub></sub> at 120 and 130 K as shown in Figure 3(a-b). It can additionally explain the blue-shift in Peak<sub>O<sub>II</sub></sub> with decrease in  $T$  beginning from 140 K rather than from 160 K. Particularly, the excitons with a large binding energy trapped in tetragonal MAPbI<sub>3</sub> during phase transition provides a potential candidate for optoelectronic device applications, especially for lasers since the exciton confinement can lower down the gain threshold.[7] Figure 4 illustrates the physical picture of the carrier transfer and recombination processes in the coexisting phases.

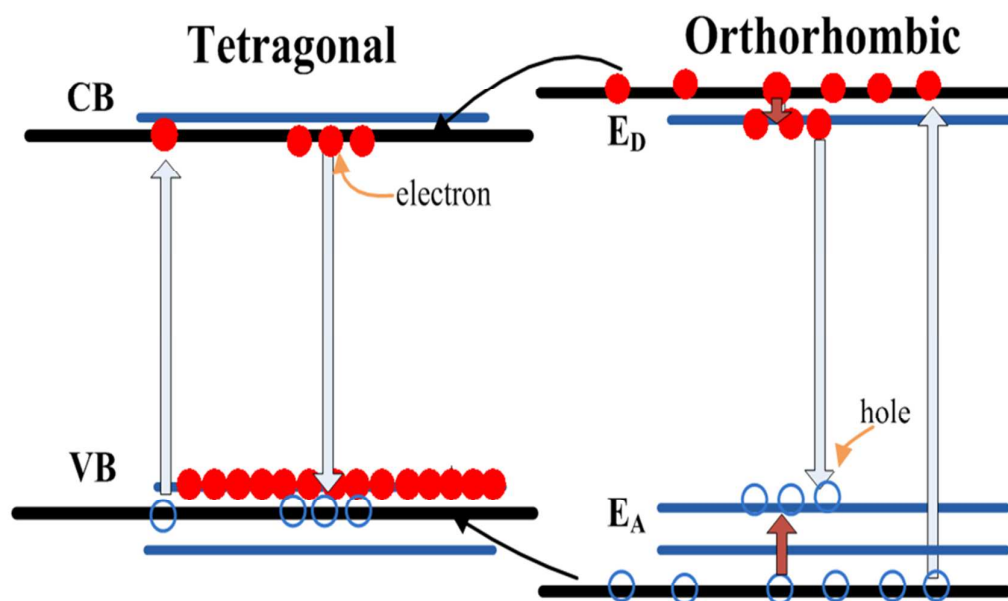


Figure 4 Diagrams schematically displaying the band structure for the two phases of the MAPbI<sub>3</sub> perovskite at 130-150 K. Excitons are confined in the tetragonal phase due to the narrower band gap of the tetragonal MAPbI<sub>3</sub>.

Since Peak<sub>OII</sub> begins to red-shift when  $T$  is lower than  $\sim 80\text{K}$ , as shown in Figure 2(b), the PL properties of the orthorhombic MAPbI<sub>3</sub> in the temperature range  $< 80\text{K}$  are further studied by performing an additional excitation-power-dependent PL measurement at  $77\text{K}$ . The results are shown in Figure 5. Due to the limited density of defect states in the crystal, the emission intensity of Peak<sub>OII</sub> exhibits a clear saturation behavior at high excitation powers, as shown in the inset of Figure 5, whereas the emission intensity of Peak<sub>OI</sub> increases almost linearly with increasing excitation power. This fact manifests the free-exciton nature of the emission labeled as Peak<sub>OI</sub>, while Peak<sub>OII</sub> denotes the emission related to defect states in the crystals, i.e. DAP related transition. Besides, as the excitation power increases from 20 to 160 mW, Peak<sub>OII</sub> blue-shifts from 783 to 777 nm. This evidence can help one to safely exclude the possibility that Peak<sub>OII</sub> originates from free-exciton recombinations of the tetragonal MAPbI<sub>3</sub>, since the blue shift in emission with the increase of the excitation power is a typical characteristic of DAP recombination.[34] At low-power excitation, low density of electrons and holes are excited by absorption of the pumping laser beam. The excited carriers can quickly relax to and are trapped by the neutral donors or acceptors, hence primarily distant DAPs recombination can occur. While at high-power excitation high density of carriers are excited, the relaxation of hot carriers leads to the filling up of the donors and acceptor energy levels, thus close DAPs recombination can be seen. The DAP-related emission thus blue shifts with the

increase of the excitation power according to Eq. (1).

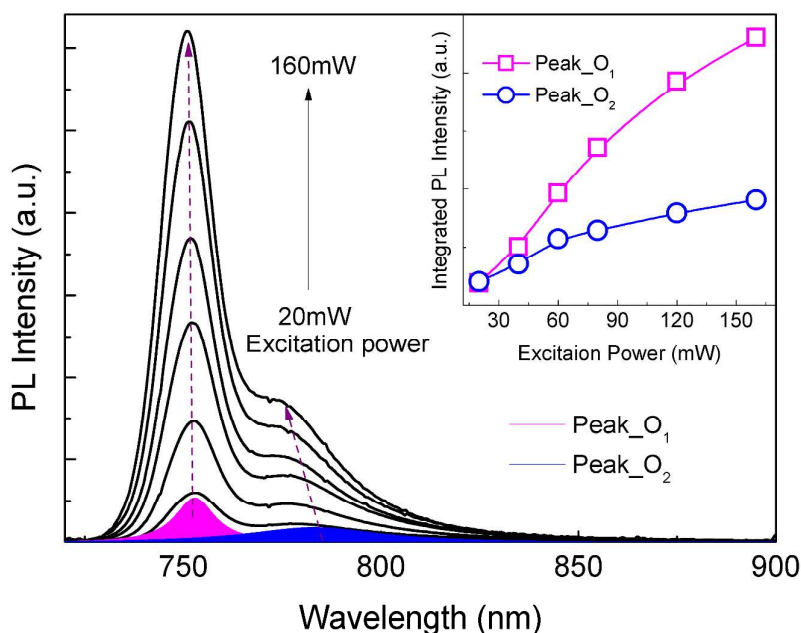


Figure 5 The excitation power dependent PL spectra of MAPbI<sub>3</sub> measured at 77 K. Peak\_O<sub>I</sub> and O<sub>II</sub> are obtained by Lorentzian deconvolution from the PL spectra of the MAPbI<sub>3</sub> which are highlighted with pink and blue, respectively. Inset: the evolution of the PL intensity for Peak\_O<sub>I, II</sub> along with increasing excitation power.

Next, we want to support our findings from PL measurements with a complementary investigation of the crystal structure by XRD measurements. Figure 6 illustrates the XRD patterns of MAPbI<sub>3</sub> crystals obtained at different temperatures. At room temperature (~300 K), the XRD peaks assigned to the (110), (220) and (330) diffraction at 14.109°, 28.461° and 43.062°, respectively, confirm the formation of a tetragonal perovskite structure with lattice parameters of  $a=c=8.866 \text{ \AA}$ ,  $b=12.668 \text{ \AA}$ . At 13 K, strong peaks at 14.359,

28.973, 32.032 and 40.909 Å, corresponding to the (101), (202), (301) and (242) diffraction, respectively, confirm the orthorhombic structure of the perovskite with lattice parameters of  $a=8.855$  Å,  $b=12.614$  Å and  $c=8.571$  Å.[1, 4, 5, 35, 36] The refined lattice parameters of the MAPbI<sub>3</sub> at different temperatures ranging from 13 to 300 K are tabulated in TABLE SI. From the XRD pattern at 150K, which is near the tetragonal-orthorhombic phase transition  $T$ , [14, 16, 33] we can clearly observe the orthorhombic phase (highlighted by asterisks). This observation indicates there is still residual tetragonal phase (highlighted by exclamation marks), although tetragonal-orthorhombic phase transition has already taken place. When  $T$  is lower than 130 K, the typical peaks from the tetragonal phase are not observed. Some factors could result in this phase coexistence, such as unequal thermal expansion and the spontaneous change of the in-plane lattice constants during the phase-transition.[12, 33] The defects in the MAPbI<sub>3</sub> crystal may also induce the phase coexistence.[37, 38] Our XRD results clearly show the coexistence of the two phases at  $T$  from 150 to 130 K. To the best of our knowledge, this is for the first time that the phase coexistence of MAPbI<sub>3</sub> around the tetragonal-orthorhombic phase transition  $T_{t-o}$  is observed through XRD, which has been predicted by previous articles.[11-13, 21]



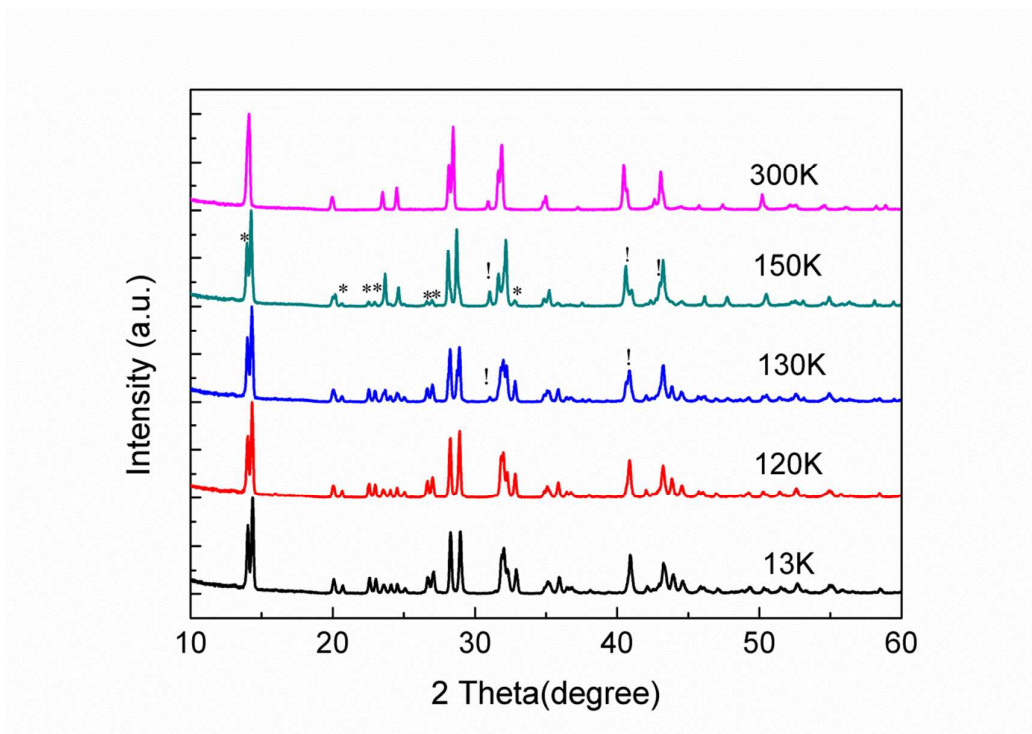


Figure 6 (a) XRD patterns of the MAPbI<sub>3</sub> at typical temperatures. The exclamation marks and asterisks are used to identify the existence of tetragonal and orthorhombic phases, respectively.

Defects in semiconductors can have an important effect on the optical and electrical properties of the crystals. Without intentional doping, MAPbI<sub>3</sub> can perform as either p or n type conductor, depending on the growth parameters.[17, 25, 30] This fact confirms the existence of intrinsic defects in the MAPbI<sub>3</sub> crystals. Unfortunately, little literature exists on the defect physics of MAPbI<sub>3</sub> around the phase transition  $T$ . [15, 18, 33] Our work shows that donors and acceptors can simultaneously exist in MAPbI<sub>3</sub> and their energy levels in the bandgap are temperature dependent. These characters could be utilized in development of novel optoelectronic devices, for example, one may tune light emission of the material via precise control of the operation

temperature of a lighting source. The phase transition is primarily induced by the angular distortions of the  $[\text{PbI}_6]$  octahedral, i.e.,  $\Gamma$  anions in  $c$  axis direction transversely displace from the mid-point of the Pb-Pb distance to which they are constrained in the ideal crystallographic description.[18, 19, 33] It is hence expected that if the DAPs are related to I or Pb, the emitting photons by the DAP recombination will give rise to a distinct shift around phase transition  $T_{t-o}$ , according to Eq. (1). This may explain the blue shift of Peak\_ O<sub>II</sub> as  $T$  decreases from 140 to 80 K. Yin et al. theoretically predicted the formation energies and the locations of the defects acting as donors and acceptors in the band structure in cubic MAPbI<sub>3</sub> perovskite.[30] According to the prediction, lead and iodine vacancies (denoted by  $V_{\text{Pb}}$ , and  $V_{\text{I}}$ , respectively) with low formation energies can be easily formed due to the strong Pb lone-pair  $s$ -orbital and I  $p$ -orbital antibonding coupling. We thus expect that Peak\_ O<sub>II</sub> observed in orthorhombic MAPbI<sub>3</sub> is related to the intrinsic defects,  $V_{\text{Pb}}$ , and  $V_{\text{I}}$ , which needs confirmation by precision calculation of theorists.

#### 4. Conclusions

In this work, we deliberately studied the abnormal luminescent properties of MAPbI<sub>3</sub> at the tetragonal-orthorhombic phase transition  $T$  ranging from 150 to 120 K. Two luminescent features upon the tetragonal-orthorhombic phase transition are observed in steady-state PL measurements. TRPL, variable-excitation-power PL, and variable-temperature XRD characterizations are performed at low temperatures to support interpretation of the origin of two

luminescent features at the phase-transition region of MAPbI<sub>3</sub>. In conclusion, our PL and XRD results unambiguously reveal the coexistence of the tetragonal and orthorhombic phase of MAPbI<sub>3</sub> in the temperature range of 150-130 K. When  $T$  is lower than 130 K, the two luminescence features observed in the orthorhombic phase originate from free excitons and DAP transitions, respectively. Our results highlight a comprehensive understanding of optical properties upon phase transition in MAPbI<sub>3</sub>, and we are confident that the findings will benefit the development of new optoelectronic devices based on perovskite materials.

**Supporting information.** Details of PL and structure properties of the MAPbI<sub>3</sub> used in this work.

### Acknowledgement

This work was sponsored by National Key Basic Research Program of China (No. 2011CB925603) and National Natural Science Foundation of China (Nos. 61290305 and 11374259). The authors would like to thank Jinke Bao for variable-temperature XRD measurement.

### References

1. Zhou, H., et al., *Photovoltaics. Interface engineering of highly efficient perovskite solar cells*. Science, 2014. **345**(6196): p. 542-6.
2. Xing, G.C., et al., *Long-Range Balanced Electron- and Hole-Transport Lengths in Organic-Inorganic CH<sub>3</sub>NH<sub>3</sub>PbI<sub>3</sub>*. Science, 2013. **342**(6156): p. 344-347.
3. Ku, Z., et al., *Full printable processed mesoscopic CH<sub>3</sub>NH<sub>3</sub>PbI<sub>3</sub>/TiO<sub>2</sub> heterojunction solar cells with carbon counter electrode*. Sci Rep, 2013. **3**: p. 3132.
4. Liu, M.Z., M.B. Johnston, and H.J. Snaith, *Efficient planar heterojunction perovskite solar cells by vapour deposition*. Nature, 2013. **501**(7467): p. 395-+.
5. Burschka, J., et al., *Sequential deposition as a route to high-performance perovskite-sensitized solar cells*. Nature, 2013. **499**(7458): p. 316-+.

6. Eperon, G.E., et al., *Formamidinium lead trihalide: a broadly tunable perovskite for efficient planar heterojunction solar cells*. Energy & Environmental Science, 2014. **7**(3): p. 982-988.
7. Xing, G.C., et al., *Low-temperature solution-processed wavelength-tunable perovskites for lasing*. Nature Materials, 2014. **13**(5): p. 476-480.
8. Wehrenfennig, C., et al., *Homogeneous Emission Line Broadening in the Organo Lead Halide Perovskite  $CH_3NH_3PbI_3-xCl_x$* . The Journal of Physical Chemistry Letters, 2014. **5**(8): p. 1300-1306.
9. Deschler, F., et al., *High Photoluminescence Efficiency and Optically Pumped Lasing in Solution-Processed Mixed Halide Perovskite Semiconductors*. The Journal of Physical Chemistry Letters, 2014. **5**(8): p. 1421-1426.
10. Kao, T.S., et al., *Lasing behaviors upon phase transition in solution-processed perovskite thin films*. Applied Physics Letters, 2014. **105**(23).
11. Yamada, Y., et al., *Near-band-edge optical responses of solution-processed organic-inorganic hybrid perovskite  $CH_3NH_3PbI_3$  on mesoporous  $TiO_2$  electrodes*. Applied Physics Express, 2014. **7**(3): p. 032302.
12. Wehrenfennig, C., et al., *Charge carrier recombination channels in the low-temperature phase of organic-inorganic lead halide perovskite thin films*. APL Materials, 2014. **2**(8): p. 081513.
13. Wu, K.W., et al., *Temperature-dependent excitonic photoluminescence of hybrid organometal halide perovskite films*. Physical Chemistry Chemical Physics, 2014. **16**(41): p. 22476-22481.
14. Fang, H.-H., et al., *Photophysics of Organic-Inorganic Hybrid Lead Iodide Perovskite Single Crystals*. Advanced Functional Materials, 2015. **25**(16): p. 2378-2385.
15. Chiarella, F., et al., *Combined experimental and theoretical investigation of optical, structural, and electronic properties of  $CH_3NH_3SnX_3$  thin films ( $X=Cl, Br$ )*. Physical Review B, 2008. **77**(4).
16. Kawamura, Y., H. Mashiyama, and K. Hasebe, *Structural study on cubic-tetragonal transition of  $CH_3NH_3PbI_3$* . Journal of the Physical Society of Japan, 2002. **71**(7): p. 1694-1697.
17. Brivio, F., A.B. Walker, and A. Walsh, *Structural and electronic properties of hybrid perovskites for high-efficiency thin-film photovoltaics from first-principles*. APL Materials, 2013. **1**(4): p. 042111.
18. Wang, Y., et al., *Density functional theory analysis of structural and electronic properties of orthorhombic perovskite  $CH_3NH_3PbI_3$* . Phys Chem Chem Phys, 2014. **16**(4): p. 1424-9.
19. Feng, J. and B. Xiao, *Crystal Structures, Optical Properties, and Effective Mass Tensors of  $CH_3NH_3PbX_3$  ( $X = I$  and  $Br$ ) Phases Predicted from HSE06*. The Journal of Physical Chemistry Letters, 2014. **5**(7): p. 1278-1282.
20. Dhanker, R., et al., *Random lasing in organo-lead halide perovskite microcrystal networks*. Applied Physics Letters, 2014. **105**(15).
21. Kao, T.S., et al., *Lasing behaviors upon phase transition in solution-processed perovskite thin films*. Applied Physics Letters, 2014. **105**(23): p. 231108.
22. Löper, P., et al., *Complex Refractive Index Spectra of  $CH_3NH_3PbI_3$  Perovskite Thin Films*

- Determined by Spectroscopic Ellipsometry and Spectrophotometry.* The Journal of Physical Chemistry Letters, 2015. **6**(1): p. 66-71.
23. Yamada, Y., et al., *Photoelectronic Responses in Solution-Processed Perovskite CH<sub>3</sub>NH<sub>3</sub>PbI<sub>3</sub> Solar Cells Studied by Photoluminescence and Photoabsorption Spectroscopy.* IEEE Journal of Photovoltaics, 2015. **5**(1): p. 401-405.
  24. Yamada, Y., et al., *Photocarrier Recombination Dynamics in Perovskite CH<sub>3</sub>NH<sub>3</sub>PbI<sub>3</sub> for Solar Cell Applications.* Journal of the American Chemical Society, 2014. **136**(33): p. 11610-11613.
  25. Stoumpos, C.C., C.D. Malliakas, and M.G. Kanatzidis, *Semiconducting Tin and Lead Iodide Perovskites with Organic Cations: Phase Transitions, High Mobilities, and Near-Infrared Photoluminescent Properties.* Inorganic Chemistry, 2013. **52**(15): p. 9019-9038.
  26. Kim, H.S., et al., *High Efficiency Solid-State Sensitized Solar Cell-Based on Submicrometer Rutile TiO<sub>2</sub> Nanorod and CH<sub>3</sub>NH<sub>3</sub>PbI<sub>3</sub> Perovskite Sensitizer.* Nano Letters, 2013. **13**(6): p. 2412-2417.
  27. Supasai, T., et al., *Formation of a passivating CH<sub>3</sub>NH<sub>3</sub>PbI<sub>3</sub>/PbI<sub>2</sub> interface during moderate heating of CH<sub>3</sub>NH<sub>3</sub>PbI<sub>3</sub> layers.* Applied Physics Letters, 2013. **103**(18): p. -.
  28. Xu, M., et al., *Highly ordered mesoporous carbon for mesoscopic CH<sub>3</sub>NH<sub>3</sub>PbI<sub>3</sub>/TiO<sub>2</sub> heterojunction solar cell.* Journal of Materials Chemistry A, 2014. **2**(23): p. 8607-8611.
  29. Yella, A., et al., *Nanocrystalline Rutile Electron Extraction Layer Enables Low-Temperature Solution Processed Perovskite Photovoltaics with 13.7% Efficiency.* Nano Letters, 2014. **14**(5): p. 2591-2596.
  30. Yin, W.-J., T. Shi, and Y. Yan, *Unusual defect physics in CH<sub>3</sub>NH<sub>3</sub>PbI<sub>3</sub> perovskite solar cell absorber.* Applied Physics Letters, 2014. **104**(6): p. 063903.
  31. D'Innocenzo, V., et al., *Excitons versus free charges in organo-lead tri-halide perovskites.* Nat Commun, 2014. **5**: p. 3586.
  32. Hamanaka, Y., et al., *Photoluminescence Properties and Its Origin of AgInS<sub>2</sub>Quantum Dots with Chalcopyrite Structure.* The Journal of Physical Chemistry C, 2011. **115**(5): p. 1786-1792.
  33. Baikie, T., et al., *Synthesis and crystal chemistry of the hybrid perovskite (CH<sub>3</sub>NH<sub>3</sub>)PbI<sub>3</sub> for solid-state sensitised solar cell applications.* Journal of Materials Chemistry A, 2013. **1**(18): p. 5628-5641.
  34. Hamanaka, Y., et al., *Luminescence properties of chalcopyrite AgInS<sub>2</sub> nanocrystals: Their origin and related electronic states.* Journal of Luminescence, 2013. **133**: p. 121-124.
  35. Heo, J.H., et al., *Efficient inorganic-organic hybrid heterojunction solar cells containing perovskite compound and polymeric hole conductors.* Nature Photonics, 2013. **7**(6): p. 486-491.
  36. Jeng, J.Y., et al., *CH<sub>3</sub>NH<sub>3</sub>PbI<sub>3</sub> Perovskite/Fullerene Planar-Heterojunction Hybrid Solar Cells.* Advanced Materials, 2013. **25**(27): p. 3727-3732.
  37. Chen, X.B., et al., *Raman analyses of co-phasing and hysteresis behaviors in V<sub>2</sub>O<sub>3</sub> thin film.* Journal of Raman Spectroscopy, 2012. **43**(12): p. 2025-2028.
  38. Schilling, P.J., et al., *Two-phase coexistence region in mechanically alloyed Cu-Fe: An X-ray absorption near-edge structure study.* Acta Materialia, 1999. **47**(8): p.

2525-2537.